




Human amniotic epithelial cell-derived extracellular vesicles provide an extracellular matrix-based microenvironment for corneal injury repair

Shuqin Hu^{1*}, Zhe Wang^{2,3*}, Caixia Jin^{1*}, Qizhen Chen⁴, Yuchen Fang⁵, Jiahui Jin¹, Jie Chen², Lixia Lu¹, Haibin Tian¹, Jingying Xu¹, Furong Gao¹, Juan Wang¹, Jieping Zhang¹, Hong-Ping Cui², Guo-Tong Xu¹ and Qingjian Ou¹ 

Abstract

To study the biological functions and applications of human amniotic epithelial cell-derived extracellular vesicles (hAEC-EVs), the cargos of hAEC-EVs were analyzed using miRNA sequencing and proteomics analysis. The hAECs and hAEC-EVs in this study had specific characteristics. Multi-omics analyses showed that extracellular matrix (ECM) reorganization, inhibition of excessive myofibroblasts, and promotion of target cell adhesion to the ECM were their primary functions. We evaluated the application of hAEC-EVs for corneal alkali burn healing in rabbits and elucidated the fundamental mechanisms. Slit-lamp images revealed that corneal alkali burns induced central epithelial loss, stromal haze, iris, and pupil obscurity in rabbits. Slit-lamp examination and histological findings indicated that hAEC-EVs facilitated re-epithelialization of the cornea after alkali burns, reduced scar formation and promoted the restoration of corneal tissue transparency. Significantly fewer α -SMA-positive myofibroblasts were observed in the hAEC-EV-treated group than the PBS group. HAEC-EVs effectively promoted the proliferation and migration of hCECs and hCSCs in vitro and activated the focal adhesion signaling pathway. We demonstrated that hAEC-EVs were excellent cell-free candidates for the treatment of ECM lesion-based diseases, including corneal alkali burns. HAEC-EVs promoted ECM reorganization and cell adhesion of target tissues or cells via orderly activation of the focal adhesion signaling pathway.

Keywords

Human amniotic epithelial cell, extracellular vesicles, corneal alkali burn, focal adhesion, extracellular matrix

Received: 31 March 2022; accepted: 29 July 2022

¹Department of Ophthalmology of Tongji Hospital and Laboratory of Clinical and Visual Sciences of Tongji Eye Institute, School of Medicine, Tongji University, Shanghai, China

²Department of Ophthalmology, Shanghai East Hospital, School of Medicine, Tongji University, Shanghai, China

³Department of Physiology, Second Military Medical University, Shanghai, China

⁴Department of Obstetrics and Gynecology, Wusong Branch, Zhongshan Hospital Fudan University, Shanghai, China

⁵Department of General Surgery, Affiliated Renhe Hospital, Shanghai University, Shanghai, China

*These authors contributed equally to this work.

Corresponding authors:

Qingjian Ou, Department of Ophthalmology of Tongji Hospital and Laboratory of Clinical and Visual Sciences of Tongji Eye Institute,

School of Medicine, Tongji University, Rm 621, Medical Bld, No.1239, Siping Rd, Shanghai 200092, China.
Email: vip@ouqingjian.com

Guo-Tong Xu, Department of Ophthalmology of Tongji Hospital and Laboratory of Clinical and Visual Sciences of Tongji Eye Institute, School of Medicine, Tongji University, Rm 623, Medical Bld, No.1239, Siping Rd, Shanghai 200092, China.
Email: gtxu@tongji.edu.cn

Hong-Ping Cui, Department of Ophthalmology, Shanghai East Hospital, School of Medicine, Rm 621, Medical Bld, No.1239, Siping Rd, Tongji University, Shanghai 200092, China.
Email: drhpcui@163.com



Introduction

The amniotic membrane is located in the inner layer of the placenta and consists of a dense amniotic epithelial cell layer that grows on the avascular stromal matrix. The innermost amniotic epithelial cells directly face the amniotic fluid and preserve the stability of the amniotic fluid environment.¹ Many studies over the past 100 years revealed that the human amniotic membrane secretes a series of growth factors and immunosuppressive factors.²⁻⁴ The human amniotic membrane also has antibacterial and anti-inflammatory properties,^{5,6} promotes wound healing and re-epithelialization,⁴ and reduces scar formation.⁷

Since 1995, amniotic membrane transplantation has been universally applied to treat ocular surface diseases, including corneal alkali burns.⁸⁻¹⁰ The cornea is positioned in the outermost eye layer and performs an important function in visual formation due to its transparent structures.^{11,12} The cornea is also susceptible to various chemical, physical, and mechanical traumas. Among these corneal traumas, corneal alkali burns are the most severe chemical ocular lesions and result in extensive corneal injury and gross impairment of the entire anterior segment of the eye.^{13,14} The treatment of corneal trauma with amniotic membrane patch transplantation is one of the most effective methods but has remained a challenging clinical problem to overcome due to its shortcomings, which include increased operative time, difficulties in amniotic membrane surgical handling, premature degeneration of the amniotic membrane, increased relative risk of surface infection and adverse calcification effects.¹⁵⁻¹⁸

Human amniotic epithelial cells (hAECs), monolayers and regular tight epithelial cells derived from amniotic membranes have become a focus in the field of regenerative medicine because of their embryonic stem cell-like proliferation and differentiation characteristics, immune modulation functions, and ease of availability.^{1,3,19,20} The administration of hAECs to animals showed sufficient effectiveness for the treatment of lung injury, liver injury and ocular surface disease with systemic safety without hemolytic reactions, toxicity or allergic reactions.²¹⁻²⁵ The paracrine factors of hAECs transplanted in vivo or cultured in vitro, independent of hAEC engraftment, attenuated myofibroblast activation, promoted macrophage polarization toward a reparative phenotype, suppressed monocyte/macrophage recruitment, and induced regulatory T cell differentiation.^{23,26,27} Extracellular vesicles (EVs) are instrumental communication vehicles that contain a variety of bioactive cargo, including cells that secrete nucleic acids, proteins, and lipids.^{28,29} Corneal stromal stem cell-derived EVs reduced inflammation and fibrosis, indicating anti-scarring effects on corneal regeneration after injury.³⁰⁻³² The effectiveness and mechanism of human amniotic epithelial cell-derived extracellular vesicles (hAEC-EVs) should not be ignored for amniotic membrane transplantation. Several studies showed that

hAEC-EVs had therapeutic effects on skin lesions,²⁶ lung injury,²² and liver disease.³³ Dermatological studies showed that hAEC-EVs promoted the healing of cutaneous wounds by increasing the migration and proliferation of fibroblasts, inhibiting excessive collagen deposition, inducing the formation of well-organized collagen fibers, and reducing scar formation in animals. However, whether hAEC-EVs may be used to treat ocular surface diseases, such as corneal alkali burns, is not known. The human amniotic membrane is widely used for the treatment of corneal trauma in clinical practice. The detailed mechanism and function of hAEC-EVs are not clear.

The present study focused on the effect and mechanism of hAEC-EVs from cultured primary hAECs to confirm the direction and field of use for hAEC-EVs in biomedicine. The hAEC-EVs were analyzed using miRNA sequencing and LC-MS/MS proteome analysis to resolve and integrate the functions and mechanisms of hAEC-EV cargoes. Topical administration of hAEC-EVs significantly alleviated corneal alkali injury in rabbits, and the effects were similar to amniotic membrane transplantation. hAEC-EVs effectively prevented excessive myofibroblast activation of corneal stromal cells, reduced scar formation and increased the re-epithelialization of corneal epithelium after corneal alkali burns. The activation of focal adhesion by hAEC-EVs on corneal cells may be a major pathway for the successful application of hAEC-EVs.

Material and methods

Human ethics

Written informed consent was obtained from each placental donor. Amniotic membranes were collected from term healthy placentas of women who underwent elective cesarean section according to the guidelines and approval of the Human Research Ethics Committee of the School of Medicine of Tongji University (Approval No. 2021tjdx053). A total of 15 placental donors were involved in this study.

Cell culture

For the isolation and culture of hAECs, the amnion was mechanically peeled from the underlying chorion and washed three times with phosphate-buffered saline (E607008, PBS, Sangon Biotech, China) supplemented with 10% penicillin and streptomycin (15070063, Thermo Fisher Scientific, USA). The amnion was incubated with 0.25% trypsin-EDTA (25200072, Thermo Fisher Scientific, USA) for 15 min at 37°C, and the human amniotic epithelial cells were mechanically detached from the amnion. Dispersed hAECs were collected via centrifugation at 1500 rpm for 10 min, plated in 10-cm cell culture dishes in DMEM/F-12 medium (11330032, Thermo Fisher Scientific, USA) supplemented with 10% fetal bovine serum (FBS, ExCell Bio, China), 10 ng/mL human

recombinant epidermal growth factor (EGF, PHG0311, Thermo Fisher Scientific, USA), 5 μ M SB431542 (301836-41-9, Selleck, China) and 1% penicillin and streptomycin, and cultured in a cell incubator at 37°C. The hAEC culture medium was changed every 2 days.

Human corneal epithelial cells (hCECs) and human corneal stromal cells (hCSCs) were a kind gift of professor Qingjun Zhou (Shandong Eye Institute, China) and cultured in DMEM/F12 medium supplemented with 10% FBS in a cell incubator at 37°C.

Isolation and identification of hAEC-EVs

HAECs at passage 3 were cultured to confluence, as shown in Figure 1(a), washed with PBS three times and cultured with DMEM/F-12 supplemented with 5% EV-depleted FBS for 48 h. The flow cytometry analysis revealed $5.93\% \pm 0.51$ apoptotic hAECs after an incubation with 5% EV-depleted FBS medium and $5.68\% \pm 0.11$ apoptosis under normal culture conditions, which was not significantly different ($p=0.44$) (Supplemental Figure 1(a)). EV-depleted FBS was obtained via the ultracentrifugation of FBS as previously described.³⁴

HAEC-EVs were isolated from the hAEC culture medium using ultracentrifugation. The collected culture medium was centrifuged at $300 \times g$ for 10 min at 4°C to eliminate the cell pellets. The supernatant was centrifuged at $2000 \times g$ for 20 min at 4°C to further remove dead cells. The supernatant was centrifuged at $10,000 \times g$ for 30 min at 4°C to remove cell debris. The supernatant was filtered through a 0.22- μ m filter (Merck, Germany), and the filtrate was transferred to new tubes and ultracentrifuged at $150,000 \times g$ for 2 h at 4°C in a SW70Ti rotor (Beckman Coulter, USA) to pellet the hAEC-EVs. The supernatant was immediately aspirated and ultracentrifuged again. The hAEC-EV pellets were resuspended in 200 μ L of cold PBS. The protein concentration of hAEC-EVs was quantified using a BCA Protein Assay Kit (BCA, 23227, Thermo Fisher Scientific, USA). The hAEC-EV particle sizes were determined using nanoparticle tracking analysis (NTA) with ZetaView PMX 110 (Particle Metrix, Meerbusch, Germany) and ZetaView 8.04.02 software. According to the NTA and BCA assays, the concentration of hAEC-EVs was 1.5×10^7 particles/ μ g.

Transmission electron microscopy (TEM, HT-7700, Hitachi, Japan) and Western blotting were performed to characterize the morphological and surface markers of hAEC-EVs.

Fluorescence-activated cell sorting analysis (FACS)

FACS of hAEC markers and apoptotic cells was performed using flow cytometry. The cultured hAECs were digested into single cells with 0.25% trypsin-EDTA and resuspended in

PBS at a final concentration of 5×10^5 cells/mL. For the analysis of hAEC markers, primary antibodies (CD29, CD73, CD326, HLA-ABC and isotype control) were added to 100 μ L of a cell suspension and incubated for 1 h at 4°C. The cells were washed twice with 2 mL PBS and centrifuged at $500 \times g$ for 5 min. For the analysis of SSEA4, the cells were fixed with 4% PFA for 5 min, permeabilized with 0.3% Triton X-100, blocked with 3% BSA for 1 h, and then sequentially incubated with the primary antibody and secondary antibody. Five hundred microliters of PBS were added to resuspend the cell pellets. For the cell apoptosis assay, hAECs were digested with 0.25% trypsin and stained in 100 μ L binding buffer with 5 μ L of Annexin V-Alexa Fluor 488 and 10 μ L of PI Staining Solution (20 μ g/mL) according to the manufacturer's instruction (40305ES20, Yeasen Biotechnology, China). All cells were analyzed using the CytoFLEX LX system (Beckman Coulter, USA). The results were evaluated using FlowJo software (Leonard Herzenberg Laboratory, USA).

Bioinformatic analysis of highly expressed miRNAs in hAEC-EVs

LC Sciences (USA) prepared the hAEC-EV miRNA-seq libraries and performed the sequencing and next-generation sequencing (NGS) data analyses. Raw reads of the library were produced using the Illumina HiSeq 2500 SE50 platform and subjected to an in-house program, ACGT101-miR (LC Sciences, USA), as described previously.³⁴ High-level miRNAs were filtered according to a higher number of reads than the average copy number of the dataset.

The relative expression of highly expressed miRNAs was visualized using the R package circlize (v0.4.13). The target genes of all highly expressed miRNAs were predicted using the R package multiMiR (v1.12.0). The package enabled retrieval of validated miRNA-target interactions from three external databases (miRecords, miRTarBase and TarBase). The genes included in at least one database were defined as target genes for specific miRNAs in this study. The protein-protein interactions (PPIs) were computed using STRING (<https://string-db.org/>), and the hub genes in the PPIs were identified using CytoHubba in Cytoscape (3.8.2). The MMC method of node centrality metrics was used to measure the importance of nodes. The top 20 target genes and 10 miRNA nodes ranked by the centrality metrics in the PPI network were considered hub genes. The target genes of the top 10 hub miRNAs were enriched using the R package clusterProfiler (v3.18.1) and were visualized using the R package ggplot2 (v3.3.5).

Proteomics analysis of hAEC-EV proteins

Total protein (50 μ g) from hAEC-EVs denatured in loading buffer and separated using SDS-PAGE (C671102, Sangon Biotech, China). The PAGE gels were stained with Coomassie brilliant blue G-250 dye (Thermo Fisher Scientific, USA), as

shown in Figure 4(a). High- and low-abundance protein bands were detected using an UltiMate[®] 3000 Nano/Capillary Autosampler (Thermo Fisher Scientific, USA) and Q Exactive Plus LCMS (Thermo Fisher Scientific, USA) (LC-MS/MS), respectively. The relative protein types and levels were determined using ProteomeDiscover 2.1 (FDR < 0.01) from the UniProt-Human database. Proteins at high and medium levels were compared and analyzed to the extracellular vesicles database (ExoCarta, <http://www.exocarta.org/>) using FunRich3.1.3.³⁵

The intersection of highly expressed proteins in three replications was visualized using the R package *venn* (v1.10). The 167 intersecting proteins were enriched using the R package *clusterProfiler* (v3.18.1), and the top 20 gene ontology (GO) terms were visualized using the R package *ggplot2* (v3.3.5). Literature-supported ligand-receptor (LR) pairs for humans were downloaded from the CellTalk Database (<http://tcm.zju.edu.cn/celltalkdb/index.php>). The LR pairs, including the 167 proteins as ligands or receptors, were used in subsequent analyses. The hub genes in these LR pairs were identified using the same method mentioned above, and the top five hub genes (ligand or receptor genes) and their interacting genes were plotted in Cytoscape (3.8.2). Each hub gene (ligand or receptor gene) and its interacting genes were enriched using the R package *clusterProfiler* (v3.18.1).

For the integrated analysis of hAEC-EV miRNAs and proteins, we mixed the target genes of miRNAs and the common highly expressed proteins to perform enrichment analyses. The top 10 GO terms, including combinations of target genes and proteins, were visualized using the R package *ggplot2* (v3.3.5). The GO terms of shared genes of target genes and the highly enriched proteins were visualized by the R package *heatmap* (v1.0.12).

Animal experiments

All animal experiments were performed in accordance with the Guide for the Care and Use of Laboratory Animals. All procedures using animal subjects were approved by the Institute of Laboratory Animal Resources of Tongji University (Approval No. TJAA09620602) and followed the ARVO statement for the use of animals in ophthalmic and vision research. Male rabbits weighing 2–2.5 kg were used in this study. A 2% sodium pentobarbital solution (1 mL/kg) was administered intravenously at the ear margin for general anesthesia, and local anesthesia was provided via the topical application of 0.5% proparacaine. At the endpoint, animals were euthanized with an overdose of intravenous pentobarbital.

For the corneal alkali burn model, ring-shaped sterile Whatman filter paper (diameter: 6 mm) (GE Healthcare Life Sciences, USA) containing 10 μ L of a 1 N NaOH solution was placed on the center of the cornea of rabbits for 20 s, as shown in Figure 2(a). The alkali-burned cornea

was immediately flushed with 40 mL of saline. A slit-lamp analysis of all ocular surfaces revealed alkali burn-induced central epithelial loss and stromal haze of the cornea, which obscured the iris and pupil (KangHuaRuiMing, China). Rabbits with corneal alkali burns were randomly divided into PBS and hAEC-EV groups ($n > 6$). The hAEC-EV group received hAEC-EV (1 mg/mL, 40 μ L) eye drops three times daily and a subconjunctival injection of hAEC-EVs (1 mg/mL, 100 μ L) twice weekly. The PBS group received 1 \times PBS instead of hAEC-EVs.

For ophthalmic examinations, the cornea was viewed and imaged using a slit lamp for the entire study to assess corneal scar haze formation. Epithelialization of the cornea was measured using fluorescein staining (Jingming, Tianjin, China). Corneal staining of sodium fluorescein was photographed using a slit lamp system (KangHuaRuiMing, China). The healing rate of the corneal epithelium was calculated based on the following formula as previously described: $100\% \times (\text{area of corneal staining at day 0} - \text{the area of staining after treatment}) / \text{area of corneal staining at day 0}$.³⁶ Corneal opacity was evaluated based on a slit lamp and classified into the following five grades as previously described: (0) completely clear; (1) iris and pupils easily visible; (2) iris and pupils still detectable; (3) pupils barely detectable; and (4) pupils invisible.³⁶

Histochemical analysis

Corneal tissue samples were fixed in a 4% paraformaldehyde (PFA, E672002-0500, Sangon Biotech, China) solution for 24 h. The tissue was paraffin embedded and cut into 3- μ m-thick sections. Hematoxylin and eosin (H&E) staining was used to analyze the pathological morphology of corneas as described in our previous study.³⁴

The distribution of collagen fibers in corneal tissue was visualized using Masson trichrome staining (BP-DL023, SenBeiJia Biological Technology Co., Ltd., China) according to the manufacturer's instructions. The sections stained with Masson trichrome staining were evaluated under a light microscope (Olympus, Japan).

Immunofluorescence assay

The expression of proteins in hAECs and corneal tissues was detected using immunofluorescence staining. The tissues were fixed in 4% PFA for 24 h, embedded in optimal cutting temperature compound, and cut into 8- μ m sections using a frozen sectioning machine (Leica, Germany). The fixed hAECs and embedded corneal tissues were labeled with primary antibodies (Supplemental Table 1) at 4°C overnight then incubated with Alexa Fluor 488/555 conjugated secondary antibodies (Supplemental Table 1) for 1 h at room temperature (RT) in the dark. The quantification of the mean fluorescence intensity was quantified with ImageJ software (NIH, USA).

Labeling and internalization assay of hAEC-EVs

Cultured hCECs or hCSCs were seeded in a 48-well plate and cultured overnight. The isolated hAEC-EVs were labeled with PKH26 (MINI26-1KT, Sigma, Germany) according to the manufacturer's instructions. Briefly, hAEC-EVs were isolated from the hAEC culture medium as described previously. The hAEC-EV pellets were resuspended in 500 μ L of Diluent C. Two microliters of PKH26 were mixed with 500 μ L of Diluent C to configure a 2 \times dye stock. The hAEC-EV pellets were rapidly dispensed into the 2 \times dye stock with immediate mixing, and then incubated 3 min at 25°C. 1 mL of 1% BSA were added and incubated for 1 min at 25°C to stop dye uptake and minimize aggregate formation. The hAEC-EV were diluted to about 25 mL with cold Dulbecco's phosphate-buffered saline (DPBS, E607009, Sangon Biotech, China) and ultracentrifuged at 150,000 \times g for 70 min at 4°C in a SW70Ti rotor to remove the excess PKH26 dye. The supernatant was immediately aspirated and ultracentrifuged again. The PKH26-labeled hAEC-EV pellets were resuspended in 200 μ L of cold DPBS. The cells were incubated in DMEM/F-12 (serum-free) supplemented with PKH26-labeled hAEC-EVs at concentrations of 25 μ g/mL total protein. After cells were incubated for 24 h, they were washed three times with PBS and fixed with 4% PFA for 10 min. Cell nuclei were stained with 4',6-diamidino-2-phenylindole (DAPI, D9542, Sigma, Germany) and observed using a confocal microscope (Leica Microsystems, Germany).

CCK-8 assay

Cultured hCECs or hCSCs were seeded on a 96-well plate at a density of 5 \times 10³ cells per well and cultured for 24 h. The culture medium was replaced with DMEM/F-12 containing hAEC-EVs at concentrations of 50 μ g/mL total protein alone or the same medium containing hAEC-EVs in combination with Y15 (T7119, TargetMol, USA). After cells were incubated for 24 h, the medium was aspirated and then freshly prepared CCK-8 (C0005, TargetMol, USA) solution was added to each well. Cell viability was measured by recording the absorbance at 450 nm with a microplate reader (iMark™ Microplate Absorbance Reader, Bio-Rad, USA), as described in our previous report.³⁷

Western blotting analysis

Corneal tissues or cultured cells were lysed using RIPA buffer (P0013B, Beyotime, China) with the addition of protease and phosphatase inhibitors (C0001 and C0004, TargetMol, USA). Twenty micrograms of total protein denatured in loading buffer (20315ES05, Yeasen, China) was separated using SDS-PAGE and transferred to a 0.45 μ m PVDF membrane (Merck, Germany). The total protein of EVs on the membrane was

stained using amido black (A8181, Sigma, Germany) as a loading control. The membranes were blocked with 5% BSA for 1 h, incubated with the primary antibodies listed in Supplemental Table 1 at 4°C overnight and incubated with horseradish peroxidase (HRP)-conjugated secondary antibodies for 2 h. Protein bands were examined using the Pierce™ ECL Western blotting substrate (32209, Thermo Fisher Scientific, USA) and a Tanon chemiluminescence image detection system (5200S, Tanon, China).

Cell proliferation assay

Cultured hCECs or hCSCs were seeded in a 48-well plate and cultured for 24 h. The cells were incubated with DMEM/F-12 (serum-free) as a control or the same medium supplemented with hAEC-EVs at concentrations of 50 μ g/mL total protein. After cells were incubated for 24 h, the 5-ethynyl-2'-deoxyuridine (EdU) cell proliferation assay was performed according to the manufacturer's instructions (EdU Cell Proliferation Kit, C0071S, Beyotime, China). The stained cells were visualized using fluorescence microscopy (Olympus, Japan).

Wound-healing migration assay

Cultured hCECs or hCSCs were passaged in 12-well plates and cultured to 80%–90% confluence. Two crossing linear scrape injuries were generated using a sterile pipette tip. The cells were incubated in DMEM/F-12 medium (serum-free) as a control or the same medium supplemented with hAEC-EVs at concentrations of 50 μ g/mL total protein. Wound closure images were acquired 0 h and 24 h after scratching. The ratio of wound healing was measured and analyzed using ImageJ (NIH, USA).

Transwell migration assay

Polycarbonate Transwell inserts with 8- μ m pore diameters were used to determine the vertical migration of hCSCs or hCECs. A volume of 500 μ L of DMEM/F-12 basal medium without FBS was added as a control or the same medium supplemented with hAEC-EVs at a concentration of 50 μ g/mL total protein was added to the lower chamber in a 24-well culture plate. Y15 (3 μ M) was added to the medium of hAEC-EVs to study the role of FAK in the hCECs or hCSCs. Cultured hCECs or hCSCs were resuspended in serum-free cell culture media, and 200 μ L of a cell solution (5 \times 10⁴ cells) was plated into the upper Transwell insert membrane. Cells were incubated for 24 h and stained with 0.5% crystal violet (60506ES60, Yeasen, China).

Images of migrating cells in the lower half of the inserts were visualized and photographed via microscopy (Olympus, Japan). Cells migrating into the lower compartment were counted in three unduplicated views per well and analyzed.

Statistical analysis

For all quantitative data, the means \pm SEM are expressed. The data were evaluated and presented using GraphPad Prism 9.0 (GraphPad Software, USA). Statistical comparisons were evaluated using one-way ANOVA. $p < 0.05$ was deemed statistically significant. Asterisks in the graphs indicate the statistical significance of the values as * $p < 0.05$, ** $p < 0.01$, and *** $p < 0.001$.

Results

Isolation and identification of hAECs and hAEC-derived EVs

Human amniotic epithelial cells (hAECs) isolated from the human amniotic membrane showed a confluent and tightly connected monolayer morphology in hAEC medium (Figure 1(a)). The hAECs at passage 3 expressed

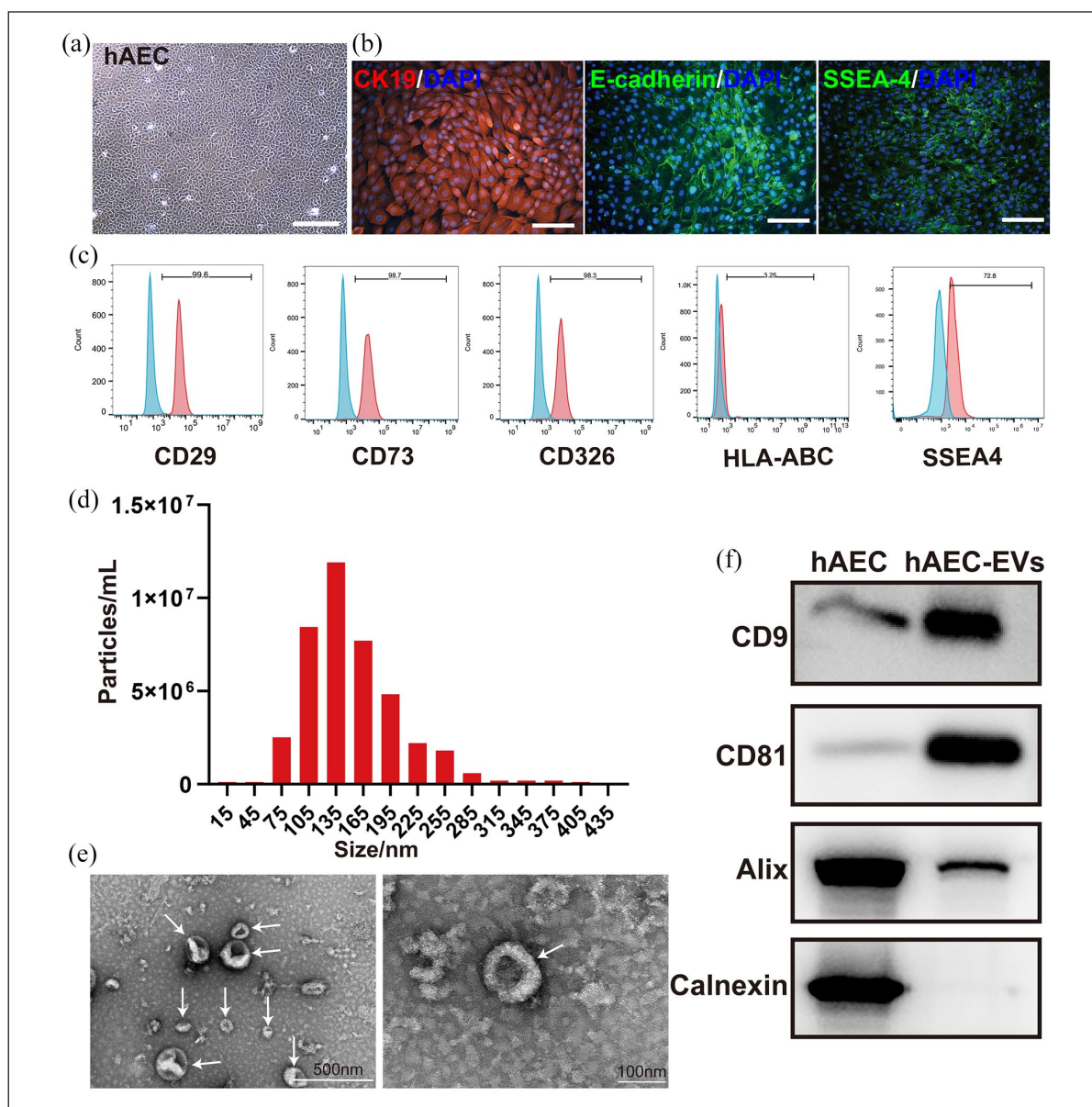


Figure 1. Isolation and identification of hAECs and hAEC-EVs. (a) Morphology of hAECs cultured in AEC medium at passage 3. Scale bar: 200 μ m. (b) Immunofluorescence staining reveals the expression of the characteristic markers CK19, E-cadherin, and SSEA4 in cultured hAECs ($n = 3$). Scale bar: 100 μ m. (c) Flow cytometry plots show that the hAECs ($n = 3$) were positive for CD29 (99.6%), CD73 (98.7%), CD326 (98.3%), and SSEA4 (72.8%) and negative for HLA-ABC (3.25%). (d) Particle size distribution of hAEC-EVs ($n = 3$) measured using nanoparticle tracking analysis (NTA). Mean = 153.6 nm, SD = 55.3 nm. (e) Morphology of hAEC-EVs ($n = 3$) was observed using transmission electron microscopy (TEM). (f) Western blot analysis of the protein profiles of hAEC-EVs ($n = 3$). hAEC whole-cell lysate was used as a control. hAECs: human amniotic epithelial cells; hAEC-EVs: hAEC-derived extracellular vesicles.

hAEC-specific markers, including CK19, E-cadherin and SSEA-4, as determined by immunofluorescence assays (Figure 1(b)). The hAECs were also positive for CD29 (99.6%), CD73 (98.7%), CD326 (98.3%), and SSEA4 (72.8%) and negative for HLA-ABC (3.25%), based on FACS analyses (Figure 1(c)). These identifications demonstrated the successful isolation and culture of hAECs.

The morphological characteristics of hAEC-EVs isolated from the hAEC culture media were analyzed using NTA and TEM. The diameters of most hAEC-EVs ranged from 105 to 195 nm and were approximately 154.5 nm on average (Figure 1(d)). The morphological assessment of hAEC-EVs using TEM revealed a typical cup-shaped morphology (Figure 1(e), Supplemental Figure 1(b)). Compared to normal hAECs, the EV-specific markers CD9, CD81, and ALIX were highly enriched in hAEC-EVs, and no calnexin expression was detected (Figure 1(f)). These data indicated that hAEC-EVs were successfully isolated from cultured hAECs and showed typical EV characteristics and statuses.

hAEC-EVs accelerate corneal recovery from alkali burns in rabbits

We treated the rabbit corneal alkali burn model with hAEC-EV resuspension to confirm the effectiveness of hAEC-EVs on corneal trauma (Figure 2(a)). We combined eye drops and subconjunctival injections to improve the retention rate of hAEC-EVs in rabbits. The corneas of rabbits with alkali burns were treated with hAEC-EVs (hAEC-EV-treated group) or PBS (control group). Normal rabbit corneas were the normal group. The corneal epithelium, which was seriously damaged with the loss of the outermost layer of the cornea, was initially re-epithelialized and involved in the recovery from corneal trauma. As shown in Figure 2(b), sodium fluorescein staining showed the loss of corneal epithelium in the central area of the cornea. The corneas treated with hAEC-EVs showed faster recovery of the corneal epithelium than the corneas treated with PBS 24 h after injury ($p < 0.05$). The epithelium of corneas treated with hAEC-EVs almost entirely recovered at 48 h, but the re-epithelialization in the PBS group was significantly slower, with a small area of corneal epithelium loss remaining ($p < 0.01$) (Figure 2(b) and (c)). The rate of corneal epithelial wound healing in the hAEC-EV group was faster than the PBS group.

The corneal stromal layer, which is the collagen-rich matrix just under the corneal epithelium, is essential to the optically transparent cornea and is easily damaged and hazed after corneal trauma. Macroscopic observations and slit-lamp photographs revealed severe scar formation and corneal haze in PBS-treated corneas 2 weeks after injury compared to the hAEC-EV-treated corneas (Figure 2(d)). The corneas treated with hAEC-EVs showed lower

corneal opacity scores than the PBS group (Figure 2(e)). These results revealed that hAEC-EVs effectively increased the re-epithelialization of the corneal epithelium and reduced scar formation of the corneal stroma after corneal alkali burns.

Histological structural analyses of the corneas were performed using H&E staining, as shown in Figure 2(f). The corneal stroma of normal rabbits showed a regular structure. Two weeks after the alkali burn, the cornea of the PBS group showed a thickened and disordered arrangement of collagen fibers, considerable infiltration of inflammatory cells and a distinct area of absent corneal keratocytes in the corneal stroma. The corneas in the hAEC-EV group were significantly thinner than the PBS group. The collagen fibers in the stroma were more densely and neatly arranged, with much lower numbers of infiltrating CD45-positive or F4/80-positive inflammatory cells in the stroma (Figure 2(f) and (g), Supplemental Figure 2). Overall, hAEC-EVs significantly promoted the re-epithelialization of the corneal epithelium and reduced scar formation of the corneal stroma after corneal alkali burns.

MiRNA sequence prediction of the function of hAEC-EV-derived miRNAs

The functional miRNAs and proteins carried by hAEC-EVs are important for hAEC-EV function in target cells. To further examine the detailed mechanisms of hAEC-EVs on corneal alkali burns, miRNA sequencing and proteomics analyses were used to identify the main cargo of hAEC-EVs.

As shown in Figure 3(a), the hAEC-EVs highly expressed miRNAs, such as hsa-miR-21-5p, hsa-miR-221-3p, hsa-miR-27b-3p, hsa-miR-200c-3p, hsa-miR-30d-5p, and hsa-miR-27a-3p, in the two donors. We analyzed all target genes of all the detected miRNAs by performing GO and Kyoto Encyclopedia of Genes and Genomes (KEGG) enrichment analyses. For the GO enrichment analysis, these miRNAs regulated processes that included cellular responses to chemical and external stress, the intrinsic apoptotic signaling pathway, myeloid cell differentiation, responses to oxidative stress and reproductive structure and system development (Supplemental Figure 3(a)). Based on the KEGG enrichment analysis, the FoxO, PI3K-Akt, p53, focal adhesion and AMPK signaling pathways were involved in the regulation of the miRNAs of hAEC-EVs (Supplemental Figure 3(b)).

To examine the key genes regulated by these miRNAs, we used three external databases (miRecords, miRTarBase and TarBase) and defined genes that were included in at least one database as target genes for each miRNA. The analyses of PPI and the MMC method revealed the top 20 hub genes in the network of gene regulation (Figure 3(b)). These hub genes included GSK3 β , KRAS, IGF1R, BCL2L11, CCND1, CASP3, EP300, STAT3, VEGFA,

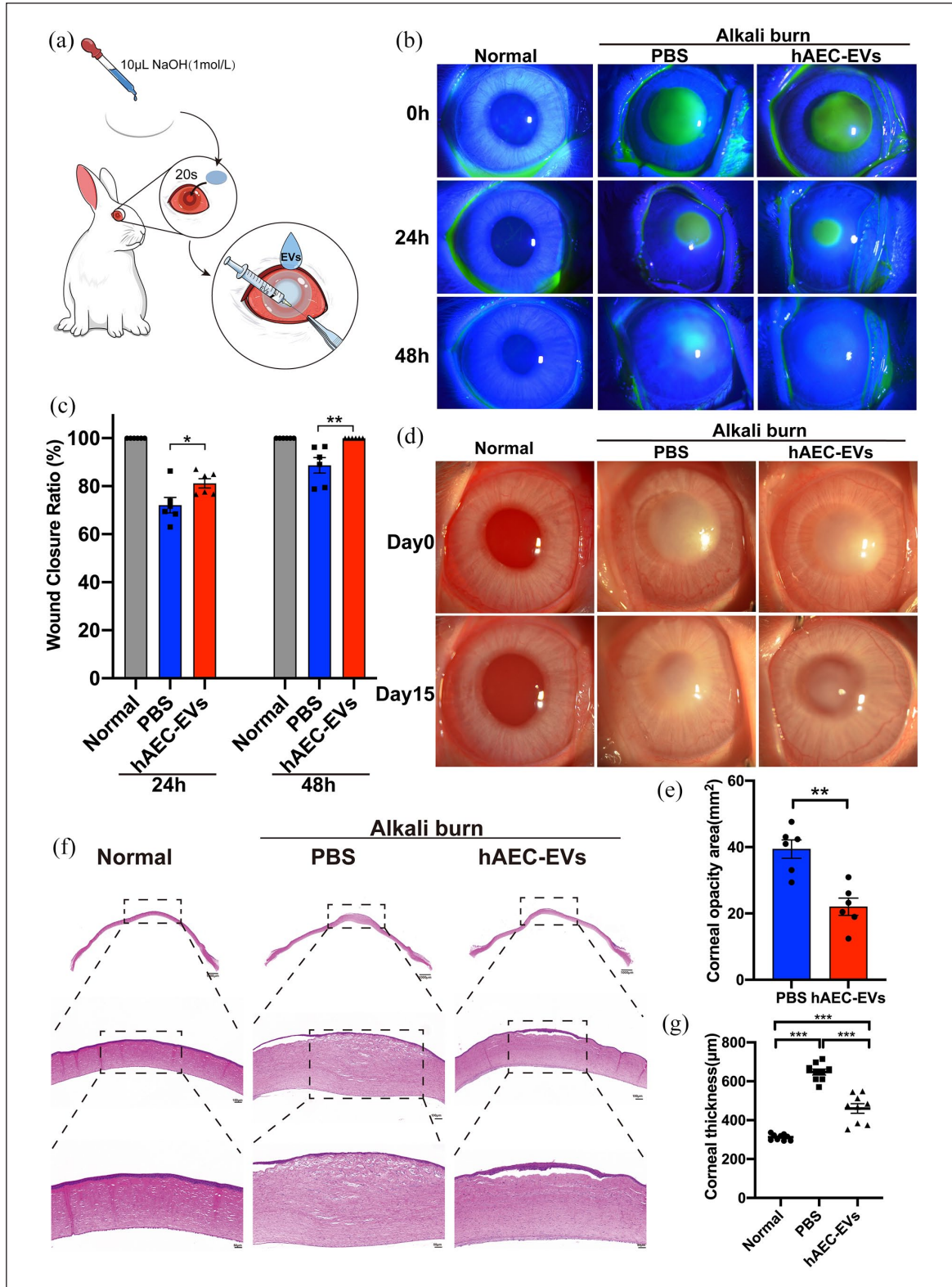


Figure 2. Application of hAEC-EVs to corneal alkali burns in rabbits. (a) Schematic showing rabbit corneal alkali burn model generation and the treatment protocol. (b and c) The corneal epithelium stained with sodium fluorescein was observed using slit-lamp for the detection of the wound closure ratio. The data are shown as the means \pm SEM ($n=6$). *: $p < 0.05$; **: $p < 0.01$. (d) The macroscopic appearances of alkali-burned eyes were photographed at different stages using a slit-lamp and direct diffuse illumination after corneal alkali burn. (e) A graph showing the corneal opacity area in hAEC-EV-treated and untreated corneas. The data are shown as the means \pm SEM ($n=6$). **: $p < 0.01$. (f and g) H&E staining of corneal sections from rabbit corneal tissue. The corneal thickness was measured using ImageJ. The data are shown as the means \pm SEM ($n=3$). ***: $p < 0.001$.

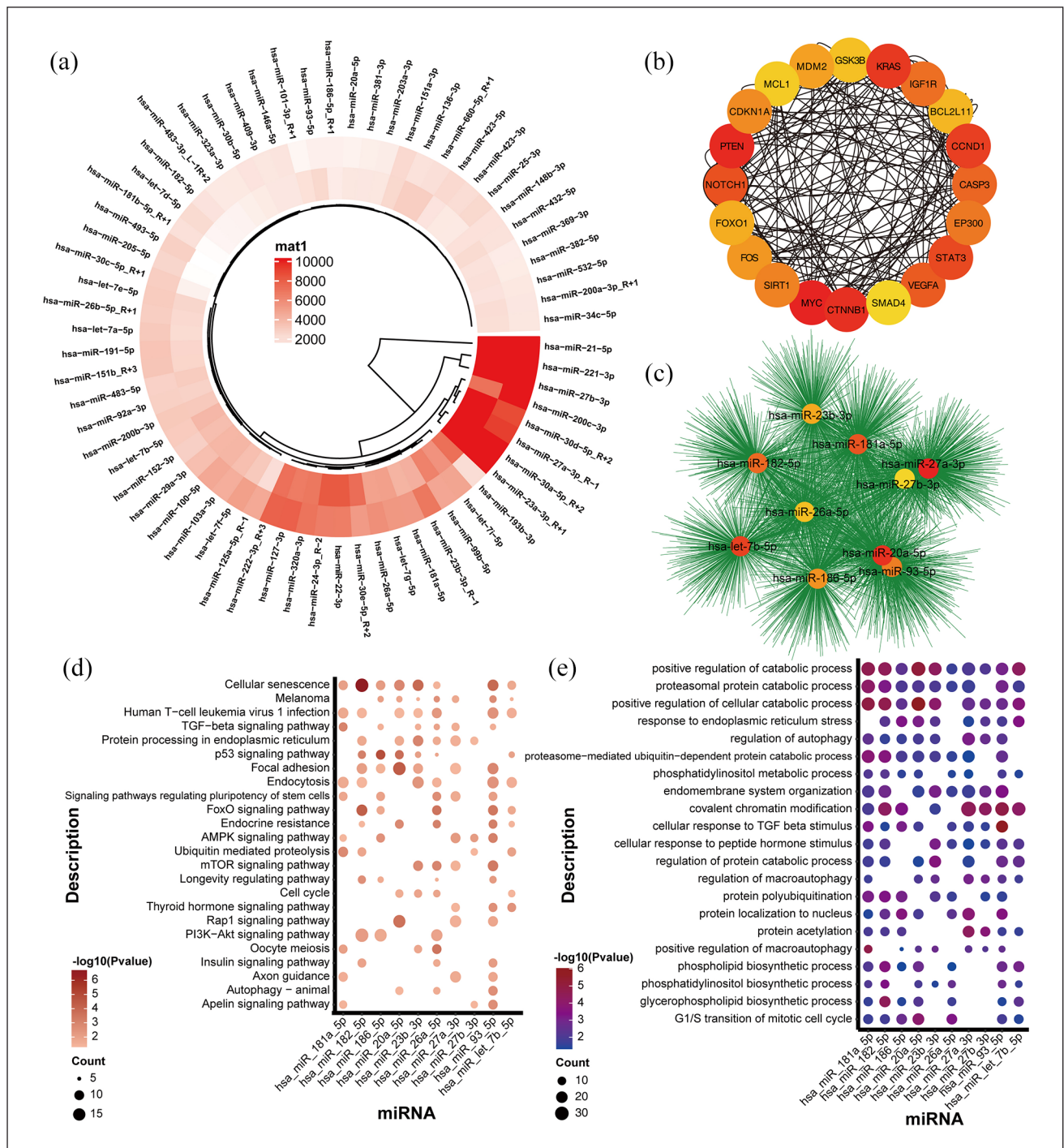


Figure 3. miRNA sequence analysis of the hAEC-EVs. (a) The relative expression levels of highly expressed miRNAs in the two donors ($n=2$). (b) The analyses of protein-protein interactions and the MMC method showed the top 20 hub genes in the network of gene regulation. (c) The top 20 miRNAs in the regulation network are shown. (d and e) The target genes of the top 10 miRNAs enriched in the KEGG signaling pathway (d) and GO enrichment (e) terms.

SMAD4, CTNNB1, MYC, SIRT1, FOS, FOXO1, NOTCH1, PTEN, CDKN1A, MCL1 and MDM2. Ten miRNAs, hsa-miR-23-3p, hsa-miR-181a-5p, hsa-miR-27a-3p, hsa-miR-27b-3p, hsa-miR-182-5p, hsa-miR-26a-5p, hsa-miR-20a-5p, hsa-let-7b-5p, hsa-miR-93-5p, and hsa-miR-186-5p, also played important roles in the regulatory

network, as shown in the PPI network analysis (Figure 3(c)). KEGG and GO enrichment analyses were applied to the common pathways and cellular processes involved in the regulation of hAEC-EVs. As shown in Figure 3(d), the target genes of these 10 miRNAs were enriched in signaling pathways, including cellular senescence, TGF β signaling,

p53 signaling, focal adhesion, FoxO signaling, and mTOR signaling pathways. GO enrichment also showed that the miRNAs regulated catabolic processes, endoplasmic reticulum stress, autophagy and macroautophagy, responses to TGF β , and protein polyubiquitination and acetylation (Figure 3(e)). Based on these analyses, we consider the hAEC-EV-derived miRNAs hsa-miR-23-3p, hsa-miR-181a-5p, hsa-miR-27a-3p, hsa-miR-27b-3p, hsa-miR-182-5p, hsa-miR-26a-5p, hsa-miR-20a-5p, hsa-let-7b-5p, hsa-miR-93-5p, and hsa-miR-186-5p as key miRNAs that intervened in the progression of corneal trauma via the TGF β signaling pathway, focal adhesion, and cellular senescence.

Proteomics analysis of the types and functions of hAEC-EV-derived proteins

We separated the total proteins of three individual hAEC-EVs using PAGE gels and analyzed the proteins using LC-MS/MS (Figure 4(a)). We compared high and medium proteins using ExoCarta, which is an exosome database that contains published exosome studies. Venn analysis revealed that 167 expressed hAEC-EV proteins intersected among the three individuals. Four types of proteins (ICOSLG, PSG1, TSPYL2, and MAP7D3) were not reported in other EV studies by Vesiclepedia (Figure 4(b)). Based on the Vesiclepedia database, most hAEC-EV proteins from the three donors were found in the placenta, ovary, liver or plasma (Figure 4(c)). GO enrichment analysis found that the proteins were enriched and involved in biological processes (protein metabolism and cell growth and/or maintenance), biological pathways (integrin family cell surface interactions, β 1 integrin cell surface interactions, and proteoglycan syndecan-mediated signaling events), cellular components (exosomes and cytoplasm), and molecular functions (extracellular matrix (ECM) structural constituent and protease inhibitor activity) (Figure 4(d)–(g)).

Because we determined the efficiency of hAEC-EVs from different donors in the rabbit alkali model, the common features of hAEC-EVs were worthy of further attention and study. We focused on the 167 common proteins shown in the Venn plot and the word cloud, and the font size was relative to the expression level (Figure 5(a) and (b)). These 167 proteins were enriched in cellular processes, including extracellular matrix organization, cell adhesion, cellular protein metabolic process, and negative regulation of endopeptidase activity (Supplemental Figure 4(a)). Several proteins (TGFBI, CD44, FN1 and TIMP2) were confirmed using Western blotting (Supplemental Figure 4(b)).

To determine the potential relationships of these proteins, PPIs were analyzed between the hub proteins (ligands or receptor genes) and their interacting genes, as shown in Figure 5(c). The hub proteins CD44, ITGB1, ITGA2, and ITGA3 are receptor genes. FN1 was the

ligand protein. The five hub proteins and their interacting proteins were primarily enriched in cellular processes, including extracellular matrix organization, cell adhesion, collagen catabolic processes, and cell migration. These processes are important for corneal recovery from trauma, especially processes related to corneal collagen remodeling.

We integrated the miRNA and proteomic analyses and showed that the 10 genes were present in the miRNA and protein analyses. Among these genes, ITGA2, ITGA3, TIMP2, LAMC1, LAMC2, and COL12A1 were related to extracellular matrix organization and extracellular structure organization (Figure 5(d)). The top 10 terms that were enriched from the mixture of miRNAs and proteins were related to extracellular matrix organization, extracellular structure organization, platelet degranulation, response to nutrient levels, myeloid cell differentiation, response to TGF β , cellular response to TGF β stimulation and the intrinsic apoptotic signaling pathway (Figure 5(e)). These analyses suggested that the interaction between ECM organization, the focal adhesion pathway, and the TGF β signaling pathway of targeted cells were the major paths of function for hAEC-EVs.

HAEC-EVs promote corneal repair via focal adhesion

HAEC-EVs may contribute to extracellular matrix reconstruction, cell adhesion and the inhibition of excessive activation of the TGF β signaling pathway. Moderate cell migration and proliferation, matrix deposition and tissue remodeling are critical for tissue recovery from most traumatic diseases, including corneal lesions, which was shown by Masson's trichrome staining of the disorganized collagen fibers of the corneal tissue in the PBS-treated group after 14 days. In contrast, the collagen fibers in the corneas of the hAEC-EV-treated group were dense and well aligned, which resembled normal corneal tissue after 14 days (Figure 6(a)). Corneas treated with PBS highly expressed α -SMA, which is related to the excessive myofibroblast transformation of corneal stromal cells. The α -SMA-positive myofibroblast cells were primarily located on the upper layer of the cornea, which was immediately next to the area of severe injury (Figure 6(b) and (c)). This situation was significantly improved with hAEC-EV treatment. The upregulation of α -SMA and connective tissue growth factor (CTGF), corneal fibrosis markers, was significantly inhibited by the hAEC-EV treatment (Figure 6(d)). Obviously, hAEC-EVs substantially alleviated the disordered extracellular matrix and stromal-sourced myofibroblast cells.

During the acute injury phase (<48 h), the corneal tissue does not have complete spontaneous repair, and the function and mechanism of hAEC-EVs are more significant to study. Based on the above omics analyses of hAEC-EVs,

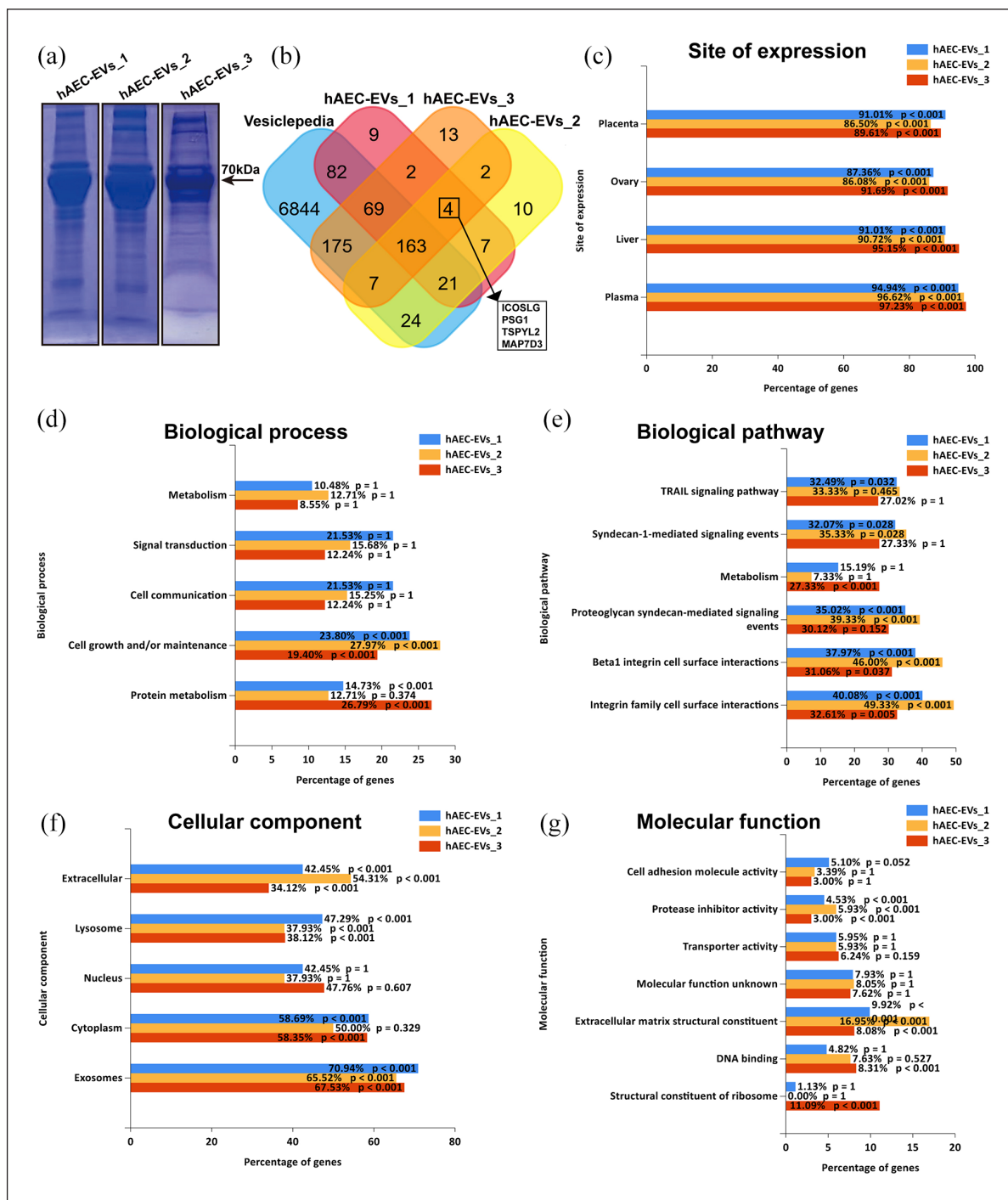


Figure 4. Proteomic analysis of the hAEC-EVs. (a) Proteins from hAEC-EVs from three donors separated using PAGE gels ($n = 3$). (b) Venn diagram showing the Vesiclepedia database and the expressed protein types of hAEC-EVs from the three donors. (c–g) FunRich analyses of the proteins of hAEC-EVs from the three donors showing overall features, including site of expression (c), biological process (d), biological pathway (e), cellular component (f), and molecular function (g).

we analyzed corneal tissues collected after hAEC-EV treatment for 24h to examine ECM replenishment and corneal stromal cell activation. As shown in Figure 6(e), ECM-related proteins, including FN1, TGFBI, TIMP2, CD44, and COLIII, which are expressed in the normal cornea and

included in hAEC-EV cargoes, were downregulated by alkali injury with PBS treatment. These proteins were significantly upregulated in corneas treated with hAEC-EVs. These data indicate that hAEC-EV cargo proteins increased the protein levels of the ECM in the injured cornea directly.

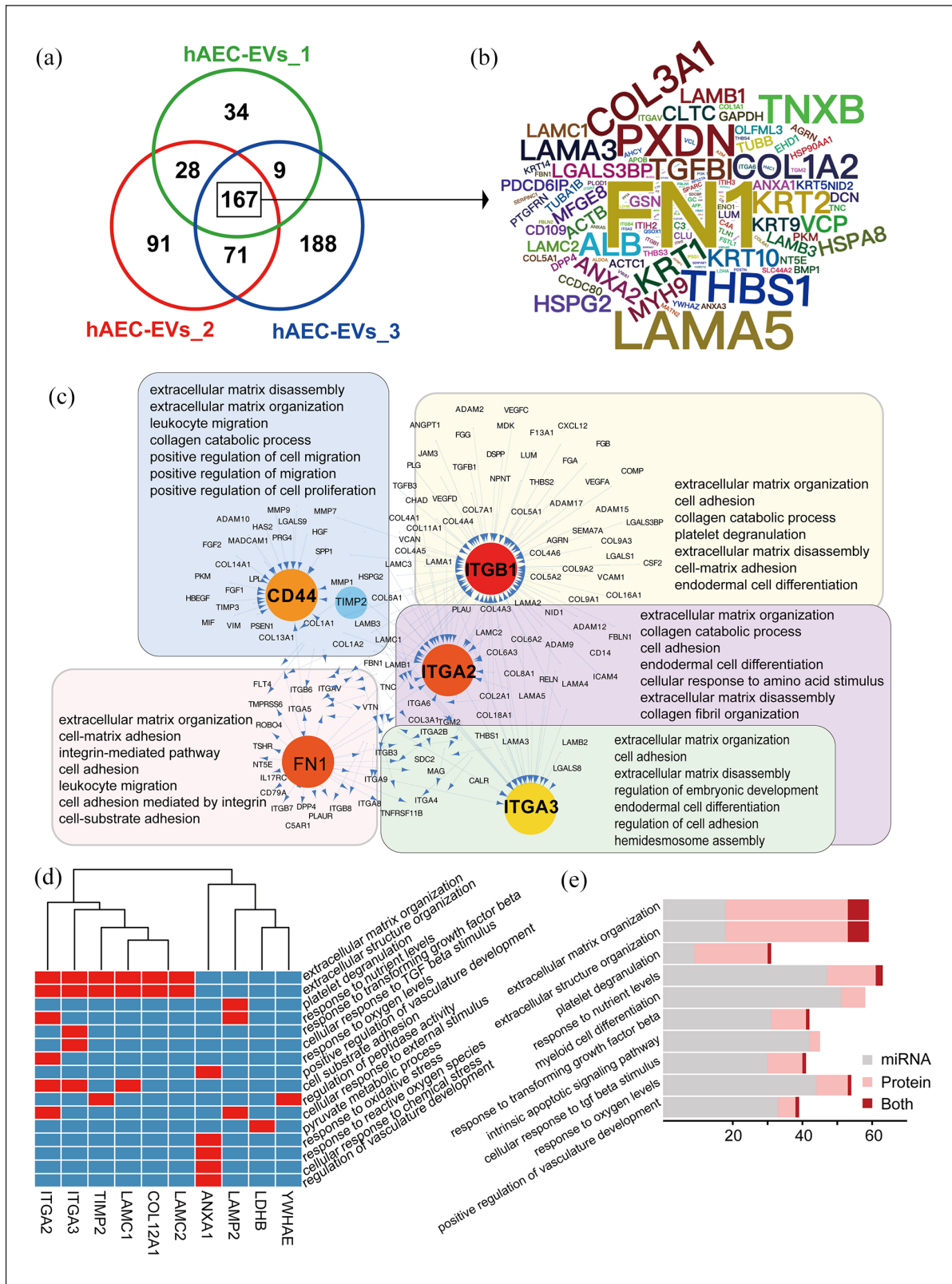


Figure 5. Integrated analysis of miRNA and proteomics of hAEC-EVs. (a) Venn diagram showing the proteins expressed in hAEC-EVs from the three donors ($n = 3$). (b) Word cloud showing the commonly expressed protein symbols of the three donors. (c) The top five hub genes of the highly enriched proteins, their ligand or receptor genes and their related GO pathways. (d) Genes that were present in miRNA and protein analyses and their corresponding GO terms. (e) The top 10 GO terms that were enriched in miRNA and protein analyses.

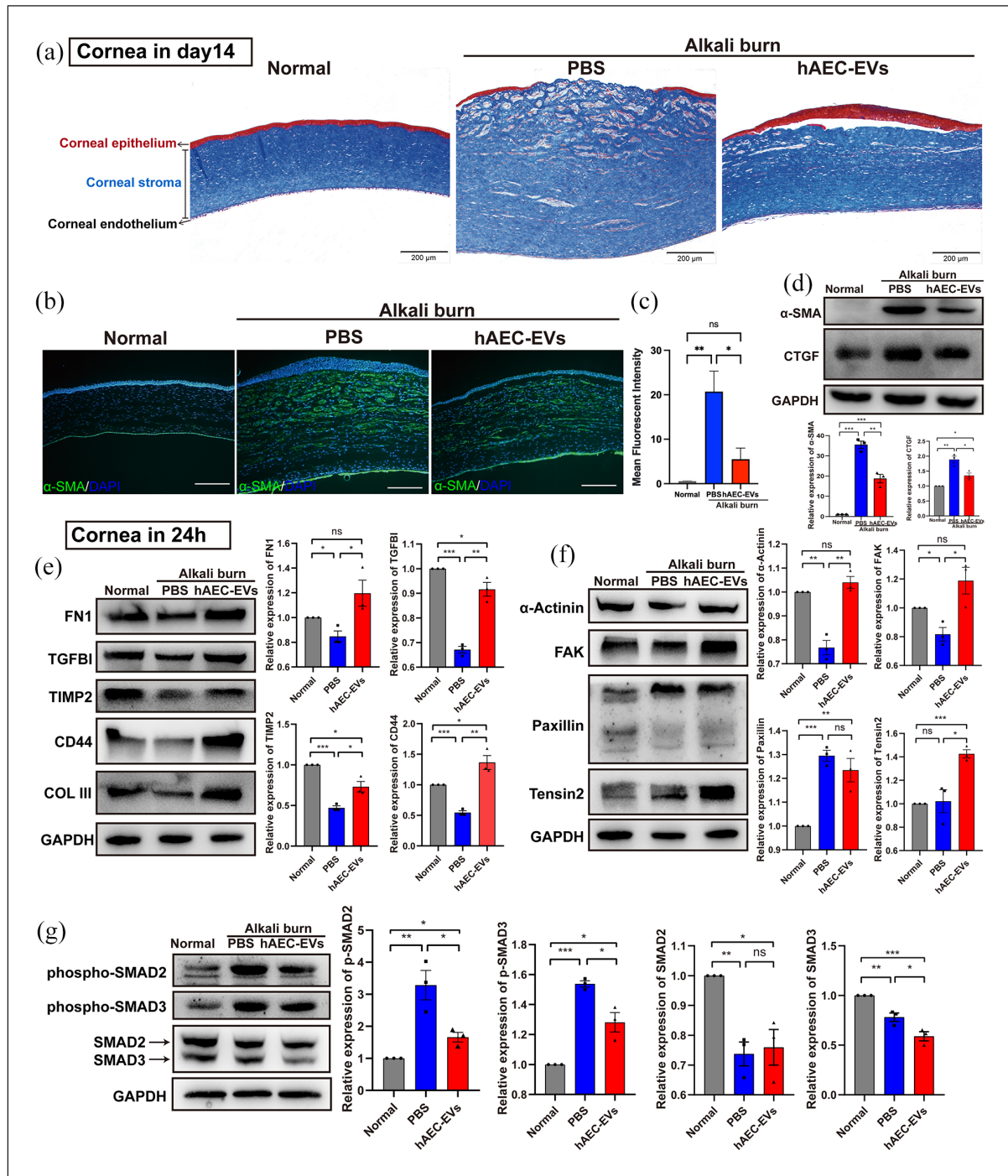


Figure 6. The mechanism of hAEC-EVs in the corneal alkali burn model. (a) Masson's trichrome staining of collagen in representative sections of rabbit corneal tissue on day 14 ($n=3$). (b) Immunofluorescence analysis of alpha-smooth muscle actin (α -SMA) in corneal sections on day 14. (c) Quantification of the mean fluorescence intensity (MFI) of α -SMA. The data are shown as the means \pm SEM ($n=3$). $**$: $p < 0.01$. (d) The protein expression of α -SMA and connective tissue growth factor (CTGF) in corneal tissue on day 14 was detected using Western blotting. The data are shown as the means \pm SEM ($n=3$). $**$: $p < 0.01$; $***$: $p < 0.001$. (e-g) Protein expression of ECM, focal adhesion and SMAD2/3 signaling in corneal tissue after treatment with PBS or hAEC-EVs for 24h.

We further explored the effect of hAEC-EVs on corneal injury and whether focal adhesion was a key process involved in the migration and adhesion of corneal cells to

the ECM. Focal adhesion kinase (FAK), which is a fundamental signaling protein regulating cell adhesion, migration, and survival, is induced and activated by the ECM.

Compared to the PBS-treated group, focal adhesion-related α -actinin, FAK, and tensin2 levels were significantly increased in the hAEC-EV-treated group. The expression of paxillin, which is involved in recruiting and binding FAK, was significantly upregulated in the PBS and hAEC-EV groups (Figure 6(f)).

TGF β -mediated SMAD2/3 signaling is first activated and involved in corneal wound healing.³⁸ However, excessive activation of TGF β promotes the myofibroblast transformation of corneal stromal cells. SMAD2 and SMAD3 in the cornea were spontaneously phosphorylated and involved in recovery from injury after 24 h in the PBS- and hAEC-EV-treated groups. The phosphorylation levels of SMAD2 and SMAD3 in the hAEC-EV-treated groups were significantly decreased compared to the PBS-treated group (Figure 6(g)). Overall, we concluded that hAEC-EVs provided ECM-related components to trigger early FAK signaling in corneal cells and attenuate excessive activation of SMAD2/3 signaling pathways to promote corneal wound healing from corneal injury in rabbits.

HAEC-EVs accelerate the proliferation and migration of hCSCs and hCECs

To further confirm the cell biological function and mechanism of hAEC-EVs on hCECs and hCSCs, we compared the cell proliferation and migration of hAEC-EVs on hCECs and hCSCs *in vitro*. HAEC-EV phagocytosis by hCECs and hCSCs was confirmed by incubating cultured cells with PKH26-labeled hAEC-EVs for 24 h. Red fluorescent particles of PKH26 were observed throughout the hCEC and hCSC cytoplasm (Supplemental Figure 5(a), 5(b)). We used an EdU assay to evaluate the effect of hAEC-EVs (50 μ g/mL) on the proliferation of hCECs and hCSCs. As shown in Figure 7(a) and (b), hAEC-EVs significantly promoted the proliferation of hCECs ($p < 0.05$) and hCSCs ($p < 0.01$) and had an on-off action on hCSCs cultured with hAEC-EVs for 24 h. The process of migration of CECs and CSCs from healthy sites to injured sites plays a vital role in corneal reconstruction after alkali injury. HAEC-EVs accelerated the migration of hCECs and hCSCs. The effect of hAEC-EVs on hCSCs was more significant than hCECs in the wound-healing assay (Figure 7(c) and (d)). Transwell migration assays revealed that hAEC-EVs promoted the migration of hCECs and activated the ability of hCSCs to migrate to the permeable membrane (Figure 7(e)). The proliferation and migration of these hCSCs and hCECs promoted by hAEC-EVs were inhibited by Y15, a focal adhesion inhibitor (Supplemental Figure 6). HAEC-EV cargo proteins (FN1 and TGFBI) were enriched in hAEC-EV-treated hCECs and hCSCs (Figure 7(f)). Therefore, hAEC-EVs promoted the proliferation and migration of hCECs and hCSCs *in vitro*.

We determined the regulation of hAEC-EV signaling in hCECs and hCSCs. To confirm whether hAEC-EVs

triggered FAK signaling in hCECs and hCSCs, as shown in our above analyses in rabbits, we analyzed the expression of focal adhesion-related proteins in hCECs and hCSCs. As shown in Figure 7(g), the phosphorylation of FAK (Tyr397) was significantly upregulated in hCECs treated with hAEC-EVs for 24 h, but it was not significantly changed in hCSCs. Activation of FAK via autophosphorylation at Tyr397 is an important early step in intracellular signal transduction triggered in response to cell interactions with the ECM. Talin-1 and paxillin, which assist in the adhesion of cells to ECMs, were significantly upregulated in hAEC-EV-treated hCSCs. In the analysis of TGF β -SMAD2/3 signaling, the phosphorylation of SMAD2 and SMAD3 was not changed in hCECs or hCSCs treated with hAEC-EVs (Supplemental Figure 7). Based on the cell biology study of hAEC-EVs *in vitro*, we considered that hAEC-EVs promoted the proliferation and migration of hCECs and hCSCs. HAEC-EVs upregulated and activated the focal adhesion signaling pathway of hCECs and hCSCs. HCECs exhibited intracellular FAK autophosphorylation, and hCSCs upregulated talin-1 and paxillin to enhance extracellular cell adhesion.

Discussion

Unlike cell transplantation, EVs isolated from stem cells are considered stem cell-based, cell-free drugs. These components are simpler to produce and have easier quality control procedures, as discussed in our previous report.³⁴ EV-related regeneration studies have shown that the ability of EVs to promote postinjury regeneration, and functional restoration was as practical as their parent cells in animals.^{39–41} It is obvious that hAEC-EVs isolated from hAECs are efficient for the treatment of corneal alkali injury and are a potential safe candidate for treating inflammation- and fibrosis-related diseases. Chemical and mechanical injury of the ocular surface are the most common and devastating ophthalmic emergencies. Chemical injuries easily penetrate the corneal stromal layer and lead to secondary complications, corneal structural disorders and blindness.⁴² Despite the adverse effects mentioned above, amniotic membrane transplantation is considered the primary clinical treatment for many severe corneal injuries. Corneal epithelial regeneration, corneal matrix deposition, inflammation reduction, inhibition of neovascularization, and prevention of corneal scar formation are the key processes for the healing of corneal lesions.⁴³ Application of hAEC-EVs to the corneal alkali burn model promoted corneal epithelial regeneration and corneal matrix deposition and alleviated inflammation. Therefore, hAEC-EVs should be a candidate treatment for corneal injury to reduce the implementation of complicated amniotic membrane transplantation.

The present study used ultracentrifugation and common characterization methods to isolate and characterize

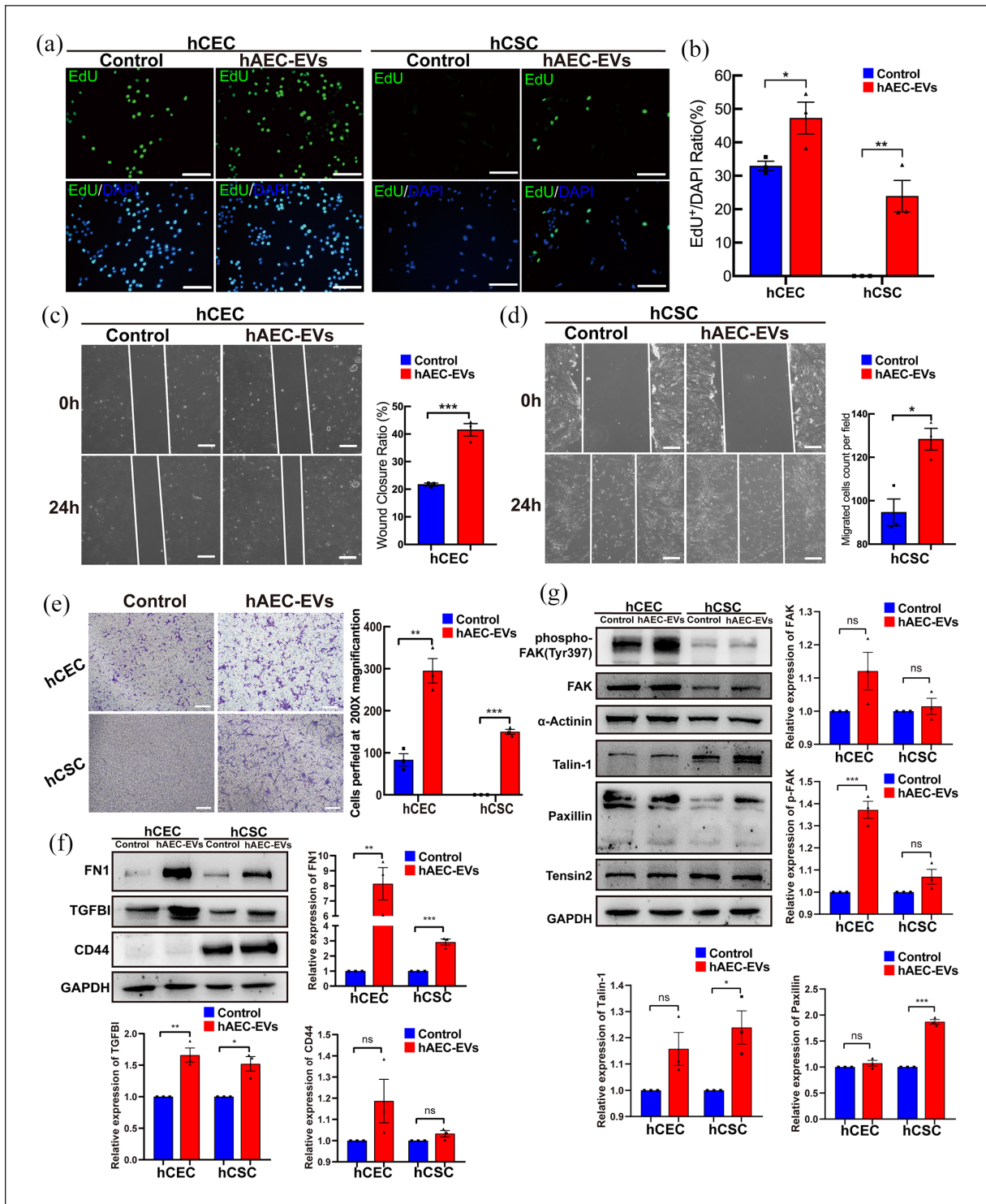


Figure 7. The facilitatory effect of hAEC-EVs on the proliferation and migration of hCECs and hCSCs. (a and b) Fluorescence images of EdU-positive staining of hCECs or hCSCs treated with PBS or hAEC-EVs (50 μ g/mL). Scale bars: 100 μ m. Histogram representing the ratio of EdU-positive stained cells (b). Data are presented as the means \pm SEM ($n=3$). * $p < 0.05$; ** $p < 0.01$. (c and d) Wound-healing assays detected the migration of hCECs (c) and hCSCs (d) treated with PBS or hAEC-EVs (50 μ g/mL). Scale bars: 200 μ m. The histogram represents the wound closure ratio. Data are presented as the means \pm SEM ($n=3$). * $p < 0.05$; *** $p < 0.001$. (e) Representative images of migrated cells with crystal violet staining in the Transwell assay for 24 h. Histogram representation of the number of migrated cells in the Transwell assay. Data are presented as the means \pm SEM ($n=3$). ** $p < 0.01$; *** $p < 0.001$. (f and g) Western blot analyses of ECM proteins (f) and focal adhesion-related proteins (g) in hCECs and hCSCs treated with PBS or hAEC-EVs. Histogram representation of the relative expression of the proteins ($n=3$). hCEC: human corneal epithelial cell; hCSC: human corneal stromal cell.

hAEC-EVs from conditioned cell culture media of hAECs.⁴⁴ However, non-EV particles, such as lipoprotein residues, are also inevitably present in EVs with current protocols.⁴⁵ Our LC-MS/MS proteomic analysis and extracellular vesicle database (Vesiclepedia) showed that this fraction of non-Vesiclepedia database reported proteins was a small fraction ($6.2\% \pm 1.3$) of hAEC-EV proteins. Although non-EV particles are present, hAEC-EVs specific proteins should play a major role in the corneal recovery. We also applied the lipophilic membrane dye PKH26, which is widely used to monitor EVs, to label the internalization of the hAEC-EVs by corneal epithelial cells and corneal stromal cells.^{46,47} The PKH26-labeled hAEC-EVs were carefully prepared to reduce non-EV-specific signaling and dye aggregation.⁴⁸ We considered several key steps and points that should be noted, including the optimal concentration of PKH26, quick preparation of the dye stock, and the use of stop reagent to avoid over-labeling. Moreover, twice more ultracentrifugation of hAEC-EVs can reduce the contamination proteins also important to reduce the non-specific binding of PKH26.

We identified the cargo (miRNA and protein) of hAEC-EVs as important paracrine components to provide a new therapeutic mechanism and potential application for the treatment of tissue damage, such as corneal alkali burns. The hAEC-EV-derived miRNAs were primarily involved in regulating cell senescence, the TGF β stimulus and signaling pathway, the p53 signaling pathway, focal adhesion, and the response to endoplasmic reticulum stress. Proteomics analysis revealed that ECM disassembly and organization, cell proliferation, and cell migration were the functions of most hAEC-EV proteins. The hAEC-EV protein functions directly improved the disease-induced hyperplasticity and disorder of the ECM. Combined analysis of the miRNAs and proteins showed that the hAEC-EVs were involved in the early regulation of the response of targeted cells to disease-induced myofibroblast activation via the TGF β signaling pathway and promoted the proliferation and migration of normal cells to repair tissue injury via ECM proteins and focal adhesion signaling. The focal adhesion signaling pathway is involved in the regulation of cell proliferation, adhesion and migration.⁴⁹ Our results showed that hAEC-EVs provided ECM and cell adhesion proteins to activate intracellular FAK signaling and increased extracellular tensin2 to promote cell adhesion and migration *in vivo*. HCECs were more sensitive to hAEC-EV phosphorylation of FAK than hCSCs *in vitro*. The ECM protein molecule TGFBI, which is an RGD-containing protein that binds to type I, II and IV collagens, is necessary in corneas. Mutant TGFBI deposited in the cornea and caused granular corneal dystrophy.⁵⁰ Early studies reported that TGFBI was a tumor suppressor, but TGFBI was recently shown to directly trigger FAK/AKT signaling to promote cell survival and migration in cancer.^{51,52} TGFBI is also important in cell-collagen interactions in the cornea, especially corneal epithelial cells. This finding explains why

hCECs easily phagocytosed and used TGFBI from hAEC-EVs to activate the phosphorylation of FAK in the present study.

Multi-omics analysis of the function and mechanism of miRNAs and proteins of hAEC-EVs revealed that hAEC-EVs can promote the cell proliferation and migration of corneal stromal cells and corneal epithelial cells. Higher dose (100 $\mu\text{g}/\text{mL}$) of hAEC-EVs more strongly promoted the cell proliferation and migration of hCSC than the dose of 50 $\mu\text{g}/\text{mL}$, but hCEC did not. The dose of 50 $\mu\text{g}/\text{mL}$ may be a saturation dose on the cell proliferation and migration of hCECs *in vitro*. In addition to the activation of fibroblasts in cutaneous skin wounds, hAEC-EVs also alleviate fibrosis in bleomycin-induced lung fibrosis⁵³ and chronic liver fibrosis.³³ This complex and sequential process of corneal reconstruction includes the death and re-population of keratocytes, the gradual transformation of keratocytes into fibroblasts and myofibroblasts, and re-shaping of the corneal ECM structure.⁵⁴ hAEC-EV-treated rabbit eyes showed lower α -SMA expression and a considerable decrease in alkali burn-induced haze and ECM deposition. Our results showed that hAEC-EVs promoted the proliferation and migration of corneal stromal cells and inhibited further differentiation of corneal stromal fibroblasts into myofibroblasts. Timely re-epithelialization is critical for preventing myofibroblast formation in the cornea.⁵⁵ ECM proteins, such as fibronectin, promote the migration of corneal epithelial cells.⁵⁶ The proliferation and migration of hCSCs showed an on-off status after treatment with hAEC-EVs *in vitro*. We noted that the miRNAs of hAEC-EVs should be involved in the regulation of fibroblasts and myofibroblasts and TGF β -SMAD2/3 signaling. It is unlikely that hAEC-EVs impact only one type of cell *in vivo*, and corneal stromal cells and corneal epithelial cells play essential roles in corneal wound healing after alkali burns.³⁶ The activation of TGF β -SMAD2/3 signaling was downregulated *in vivo*. hAEC-EVs did not significantly affect TGF β -SMAD2/3 signaling in hCSCs or hCECs *in vitro*, which may be because these two cell lines have high background activation levels of SMAD2/3 for expansion *in vitro*. Therefore, several beneficial effects of hAEC-EVs on corneal wound healing may directly activate corneal stromal cell proliferation and migration by providing ECM proteins, activating the focal adhesion signaling pathway and improving the microenvironment of the corneal injury area.

Our findings elucidate the detailed mechanism of amniotic membrane transplantation based on hAEC-EVs and confirmed the use of hAEC-EVs in corneal trauma. hAEC-EVs regulated the excessive activation of the TGF β signaling pathway via miRNAs and provided ECM proteins to reconstruct the microenvironment of lesions and trigger FAK signaling to promote cell survival and migration in corneal wound healing. For other applications, we consider hAEC-EVs good cell-free drugs for acute-phase fibrotic diseases, such as COVID-19-induced fibrotic lung parenchymal remodeling,

which is characterized by fibroblast proliferation, airspace obliteration, and micro-honeycombing.⁵⁷ However, additional potential issues should be considered in further studies, including whether the use of hAEC-EVs at a later stage will reduce scarring and methods to improve the sustainability of hAEC-EVs. We hope that hAEC-EVs will be a viable candidate for tissue restoration involving ECM reorganization in the future.

Conclusions

HAEC-EVs provided functional miRNAs and proteins to the wound area of alkali-burned rabbit corneas and promoted rapid re-epithelialization of the corneal epithelium, initiation of the proliferation and migration of corneal stromal cells, and orderly regeneration of the corneal stroma collagen. Based on our findings, hAEC-EVs may be an effective treatment for promoting tissue restoration involving ECM reorganization and inhibition of excessive myofibroblast activation, including corneal injury.

Acknowledgements

We acknowledge professor Qingjun Zhou (Shandong Eye Institute, China) for the kind gifts of the human corneal epithelial cell line and human corneal stromal cell line.

Authors' contributions

SH, CJ, and QO conceived and designed the experiments, performed the experiments, analyzed the data, and wrote the paper. ZW and QO collected and analyzed the miRNA-seq data and proteomics data. QO, G-TX, and H-PC contributed to designing the experiment, obtaining financial support, and writing the manuscript and provided final approval of the manuscript. QC, YF, JC, and JJ performed the experiments. HT, JX, FG, JW, LL, and JZ contributed reagents/materials/analytical tools. All authors have read and approved the manuscript.

Declaration of conflicting interests

The author(s) declared no potential conflicts of interest with respect to the research, authorship, and/or publication of this article.

Funding

The author(s) disclosed receipt of the following financial support for the research, authorship, and/or publication of this article: This study was supported by grants from the National Natural Science Foundation of China (32070719, 81770942, and 81870634) and the Postdoctoral Science Foundation of China (2019M661631).

Ethical approval

After written informed consent was obtained from every placental donor, amniotic membranes were collected from term healthy placentas of women who underwent elective cesarean section

according to the guidelines and approval of the Human Research Ethics Committee of the School of Medicine of Tongji University (Approval No. 2021TJDX053). All animal procedures were performed according to the institutional guidelines and the Guide for the Care and Use of Laboratory Animals issued by the NIH and the guidelines of the Animal Experimentation Ethics Committee of Tongji University (Approved No. TJAA09620602), as well as the Association for Research in Vision and Ophthalmology Statement for the Use of Animals in Ophthalmic and Vision Research.

ORCID iD

Qingjian Ou  <https://orcid.org/0000-0002-6881-8680>

Supplemental material

Supplemental material for this article is available online.

Availability of data and materials

miRNA-seq data generated in the study can be accessed at the Gene Expression Omnibus under accession code GSE190250 (<https://www.ncbi.nlm.nih.gov/geo/query/acc.cgi?acc=GSE190250>). The mass spectrometry proteomics data have been deposited to the ProteomeXchange Consortium (<http://proteomecentral.proteomexchange.org>) via the iProX partner repository with the dataset identifier PXD030221 (<http://proteomecentral.proteomexchange.org/cgi/GetDataset?ID=PX030221>). All other data are included within the article and its additional files.

References

- Zhang Q and Lai D. Application of human amniotic epithelial cells in regenerative medicine: a systematic review. *Stem Cell Res Ther* 2020; 11(1): 439.
- Li JY, Ren KK, Zhang WJ, et al. Human amniotic mesenchymal stem cells and their paracrine factors promote wound healing by inhibiting heat stress-induced skin cell apoptosis and enhancing their proliferation through activating PI3K/AKT signaling pathway. *Stem Cell Res Ther* 2019; 10(1): 247.
- Li H, Niederkorn JY, Neelam S, et al. Immunosuppressive factors secreted by human amniotic epithelial cells. *Investig Ophthalmol Vis Sci* 2005; 46(3): 900–907.
- Koizumi NJ, Inatomi TJ, Sotozono CJ, et al. Growth factor mRNA and protein in preserved human amniotic membrane. *Curr Eye Res* 2000; 20(3): 173–177.
- Talmi YP, Sigler L, Inge E, et al. Antibacterial properties of human amniotic membranes. *Placenta* 1991; 12(3): 285–288.
- Solomon A, Rosenblatt M, Monroy D, et al. Suppression of interleukin 1alpha and interleukin 1beta in human limbal epithelial cells cultured on the amniotic membrane stromal matrix. *Br J Ophthalmol* 2001; 85(4): 444–449.
- Tseng SC, Li DQ and Ma X. Suppression of transforming growth factor-beta isoforms, TGF-beta receptor type II, and myofibroblast differentiation in cultured human corneal and limbal fibroblasts by amniotic membrane matrix. *J Cell Physiol* 1999; 179(3): 325–335.
- Shanbhag SS, Hall L, Chodosh J, et al. Long-term outcomes of amniotic membrane treatment in acute Stevens-Johnson syndrome/toxic epidermal necrolysis. *Ocul Surf* 2020; 18(3): 517–522.

9. Nazari Hashemi P, Chaventre F, Bisson A, et al. Mapping of proteomic profile and effect of the spongy layer in the human amniotic membrane. *Cell Tissue Bank* 2020; 21(2): 329–338.
10. Meller D, Pauklin M, Thomasen H, et al. Amniotic membrane transplantation in the human eye. *Dtsch Arztebl Int* 2011; 108(14): 243–248.
11. Ludwig PE, Huff TJ and Zuniga JM. The potential role of bioengineering and three-dimensional printing in curing global corneal blindness. *J Tissue Eng* 2018; 9: 2041731418769863.
12. Tokuda Y, Okumura N, Komori Y, et al. Transcriptome dataset of human corneal endothelium based on ribosomal RNA-depleted RNA-Seq data. *Sci Data* 2020; 7(1): 407.
13. Joubert R, Daniel E, Bonnin N, et al. Retinoic acid engineered amniotic membrane used as graft or homogenate: positive effects on corneal alkali burns. *Investig Ophthalmol Vis Sci* 2017; 58(9): 3513–3518.
14. Xu W, Wang Z, Liu Y, et al. Carboxymethyl chitosan/gelatin/hyaluronic acid blended-membranes as epithelia transplanting scaffold for corneal wound healing. *Carbohydr Polym* 2018; 192: 240–250.
15. Shayan Asl N, Nejat F, Mohammadi P, et al. Amniotic membrane extract eye drop promotes limbal stem cell proliferation and corneal epithelium healing. *Cell J* 2019; 20(4): 459–468.
16. Guo Q, Hao J, Yang Q, et al. A comparison of the effectiveness between amniotic membrane homogenate and transplanted amniotic membrane in healing corneal damage in a rabbit model. *Acta Ophthalmol* 2011; 89(4): e315–e319.
17. Sangwan VS, Burman S, Tejwani S, et al. Amniotic membrane transplantation: a review of current indications in the management of ophthalmic disorders. *Indian J Ophthalmol* 2007; 55(4): 251–260.
18. Tseng SCG, Espana EM, Kawakita T, et al. How does amniotic membrane work? *Ocul Surf* 2004; 2(3): 177–187.
19. Miki T, Lehmann T, Cai H, et al. Stem cell characteristics of amniotic epithelial cells. *Stem Cells* 2005; 23(10): 1549–1559.
20. Miki T. Amnion-derived stem cells: in quest of clinical applications. *Stem Cell Res Ther* 2011; 2(3): 25.
21. Yang PJ, Yuan WX, Liu J, et al. Biological characterization of human amniotic epithelial cells in a serum-free system and their safety evaluation. *Acta Pharmacol Sin* 2018; 39(8): 1305–1316.
22. Hodges RJ, Lim R, Jenkin G, et al. Amnion epithelial cells as a candidate therapy for acute and chronic lung injury. *Stem Cells Int* 2012; 2012: 709763.
23. Andrewartha N and Yeoh G. Human amnion epithelial cell therapy for chronic liver disease. *Stem Cells Int* 2019; 2019: 8106482.
24. Zhao B, Liu JQ, Zheng Z, et al. Human amniotic epithelial stem cells promote wound healing by facilitating migration and proliferation of keratinocytes via ERK, JNK and AKT signaling pathways. *Cell Tissue Res* 2016; 365(1): 85–99.
25. Parmar DN, Alizadeh H, Awwad ST, et al. Ocular surface restoration using non-surgical transplantation of tissue-cultured human amniotic epithelial cells. *Am J Ophthalmol* 2006; 141(2): 299–307.
26. Zhao B, Zhang Y, Han S, et al. Exosomes derived from human amniotic epithelial cells accelerate wound healing and inhibit scar formation. *J Mol Histol* 2017; 48(2): 121–132.
27. Zhao B, Li X, Shi X, et al. Exosomal MicroRNAs derived from human amniotic epithelial cells accelerate wound healing by promoting the proliferation and migration of fibroblasts. *Stem Cells Int* 2018; 2018: 5420463.
28. Colao IL, Corteling R, Bracewell D, et al. Manufacturing exosomes: a promising therapeutic platform. *Trends Mol Med* 2018; 24(3): 242–256.
29. Roefs MT, Sluijter JPG and Vader P. Extracellular vesicle-associated proteins in tissue repair. *Trends Cell Biol* 2020; 30(12): 990–1013.
30. Kumar A, Yun H, Funderburgh ML, et al. Regenerative therapy for the cornea. *Prog Retin Eye Res* 2022; 87: 101011.
31. Yam GH, Yang T, Geary ML, et al. Human corneal stromal stem cells express anti-fibrotic microRNA-29a and 381-5p - a robust cell selection tool for stem cell therapy of corneal scarring. *J Adv Res* 2022. DOI: 10.1016/j.jare.2022.05.008.
32. Kumar A, Li Y, Mallick S, et al. *Stem Cell Secretome Promotes Scarless Corneal Wound Healing and Rescues Corneal Sensory Nerves*. bioRxiv, 2022: DOI: 10.1101/2022.05.07.490347.
33. Alhomrani M, Correia J, Zavou M, et al. The human amnion epithelial cell secretome decreases hepatic fibrosis in mice with chronic liver fibrosis. *Front Pharmacol* 2017; 8: 748.
34. Jin J, Ou Q, Wang Z, et al. BMSC-derived extracellular vesicles intervened the pathogenic changes of scleroderma in mice through miRNAs. *Stem Cell Res Ther* 2021; 12(1): 327.
35. Pathan M, Keerthikumar S, Chisanga D, et al. A novel community driven software for functional enrichment analysis of extracellular vesicles data. *J Extracell Vesicles* 2017; 6(1): 1321455.
36. Liu N, Zhang X, Li N, et al. Tetrahedral framework nucleic acids promote corneal epithelial wound healing in vitro and in vivo. *Small* 2019; 15(31): e1901907.
37. Jin C, Ou Q, Chen J, et al. Chaperone-mediated autophagy plays an important role in regulating retinal progenitor cell homeostasis. *Stem Cell Res Ther* 2022; 13(1): 136.
38. Hutcheon AE, Guo XQ, Stepp MA, et al. Effect of wound type on Smad 2 and 4 translocation. *Investig Ophthalmol Vis Sci* 2005; 46(7): 2362–2368.
39. Doepfner TR, Herz J, Görgens A, et al. Extracellular vesicles improve post-stroke neuroregeneration and prevent postischemic immunosuppression. *Stem Cells Transl Med* 2015; 4(10): 1131–1143.
40. Kim DK, Nishida H, An SY, et al. Chromatographically isolated CD63+CD81+ extracellular vesicles from mesenchymal stromal cells rescue cognitive impairments after TBI. *Proc Natl Acad Sci U S A* 2016; 113(1): 170–175.
41. Zhang J, Guan J, Niu X, et al. Exosomes released from human induced pluripotent stem cells-derived MSCs facilitate cutaneous wound healing by promoting collagen synthesis and angiogenesis. *J Transl Med* 2015; 13: 49.
42. Baradaran-Rafii A, Eslani M, Haq Z, et al. Current and upcoming therapies for ocular surface chemical injuries. *Ocul Surf* 2017; 15(1): 48–64.

43. Sharma N, Kaur M, Agarwal T, et al. Treatment of acute ocular chemical burns. *Surv Ophthalmol* 2018; 63(2): 214–235.
44. Gardiner C, Di Vizio D, Sahoo S, et al. Techniques used for the isolation and characterization of extracellular vesicles: results of a worldwide survey. *J Extracell Vesicles* 2016; 5: 32945.
45. Mathieu M, Martin-Jaular L, Lavieu G, et al. Specificities of secretion and uptake of exosomes and other extracellular vesicles for cell-to-cell communication. *Nat Cell Biol* 2019; 21(1): 9–17.
46. Kumar A, Sundaram K, Mu J, et al. High-fat diet-induced upregulation of exosomal phosphatidylcholine contributes to insulin resistance. *Nat Commun* 2021; 12(1): 213.
47. Song Y, Li Z, He T, et al. M2 microglia-derived exosomes protect the mouse brain from ischemia-reperfusion injury via exosomal miR-124. *Theranostics* 2019; 9(10): 2910–2923.
48. Takov K, Yellon DM and Davidson SM. Confounding factors in vesicle uptake studies using fluorescent lipophilic membrane dyes. *J Extracell Vesicles* 2017; 6(1): 1388731.
49. Bauer MS, Baumann F, Daday C, et al. Structural and mechanistic insights into mechanoactivation of focal adhesion kinase. *Proc Natl Acad Sci U S A* 2019; 116(14): 6766–6774.
50. Han KE, Choi SI, Kim TI, et al. Pathogenesis and treatments of TGFBI corneal dystrophies. *Prog Retin Eye Res* 2016; 50: 67–88.
51. Han B, Cai H, Chen Y, et al. The role of TGFBI (β ig-H3) in gastrointestinal tract tumorigenesis. *Mol Cancer* 2015; 14: 64.
52. Corona A and Blobe GC. The role of the extracellular matrix protein TGFBI in cancer. *Cell Signal* 2021; 84: 110028.
53. Tan JL, Lau SN, Leaw B, et al. Amnion epithelial cell-derived exosomes restrict lung injury and enhance endogenous lung repair. *Stem Cells Transl Med* 2018; 7(2): 180–196.
54. Ljubimov AV and Saghizadeh M. Progress in corneal wound healing. *Prog Retin Eye Res* 2015; 49: 17–45.
55. Nakamura K, Kurosaka D, Yoshino M, et al. Injured corneal epithelial cells promote myodifferentiation of corneal fibroblasts. *Investig Ophthalmol Vis Sci* 2002; 43(8): 2603–2608.
56. Nishida T, Nakagawa S, Awata T, et al. Fibronectin promotes epithelial migration of cultured rabbit cornea in situ. *J Cell Biol* 1983; 97(5): 1653–1657.
57. Grillo F, Barisione E, Ball L, et al. Lung fibrosis: an undervalued finding in COVID-19 pathological series. *Lancet Infect Dis* 2021; 21(4): e72.